hydrogen

MDPI

Article

Double-Hybrid Density Functional Theory Investigation of $MgScH_n$ and $MgTiH_n$ Clusters ($n \leq 18$)

Jonathan T. Lyon

Department of Chemistry, Murray State University, Murray, KY 42071, USA; jlyon6@murraystate.edu; Tel.: +1-270-809-5378

Abstract

Transition metal-doped magnesium hydride solids are leading candidates as hydrogen storage materials. Here, a double-hybrid density functional theory method is used for the first time to explore the ground state geometries and electronic properties of small $MgScH_n$ and $MgTiH_n$ (n = 1–18) clusters. It is determined that hydrogen atoms aggregate to the metal core of the cluster up to a saturation limit of $MgScH_{13}$ and $MgTiH_{14}$ for each transition metal. Additional hydrogen atoms exist as weakly interacting dissociated H_2 molecules. These saturated clusters containing scandium and titanium contain a large hydrogen mass percent of 15.9% and 16.4%, respectively. A detailed discussion of cluster growth mechanisms, hydrogen dissociation pathways, the effect of each different transition metal, and the cluster stabilities is presented as determined at the DSDPBEP86/6-311++G(3df,3pd) level of theory.

Keywords: clusters; double-hybrid density functional theory; Møller–Plesset perturbation; global optimization; doped magnesium hydride; solid-state material; hydrogen storage; hydrogen desorption

1. Introduction

The world's dependence for decades on fossil fuels as a primary energy source is leading to severe environmental strains, including air pollution and global warming, and major health issues in our current population [1,2]. In the search for an alternative energy source to help replace fossil fuels, hydrogen is a very promising candidate [3–5]. It is light, has a high energy density and, perhaps most important, is a clean energy source producing water as a byproduct when burnt in oxygen. However, H_2 is a gas at ambient temperatures and pressures, and using gases requires special equipment and additional safety and handling considerations. To elevate this, alternative ways of storing hydrogen more safely for use as an energy source are an active focus of discussion and research. Liquefying H_2 requires cryogenic temperatures, which has unique safety and handling concerns of its own. Physisorption of hydrogen on a substrate also often requires extreme cold temperatures, given the inert nature of H_2, and has a limit to the hydrogen coverage that can be accumulated. Hydrogen can be stored as a chemical hydride (e.g., methanol), but this often requires high temperatures and expensive catalysts to extract H_2 by sophisticated chemical reactions. However, storing hydrogen as a solid metal hydride is a viable option as a reversible hydrogen storage material [6,7]. While simple binary metal hydrides often have the form of MH or MH_2 ionic compounds, many other ratios between metal and hydrogen atoms exist for more complex hydrides and solid materials. Here, we define a

Check for updates

Academic Editor: Andrea Rossin

Received: 24 April 2026
Revised: 21 May 2026
Accepted: 24 May 2026
Published: 2 June 2026

Copyright: © 2026 by the author. Licensee MDPI, Basel, Switzerland. This article is an open access article distributed under the terms and conditions of the Creative Commons Attribution (CC BY) license.

hydride as any species containing hydrogen, and typically hydrogen carries a net negative charge in binary metal hydrides.

Of the various possible metal hydrides, MgH_2 shows promise, as magnesium has the advantages of being light, non-toxic, abundant, and inexpensive. The largest issue with using magnesium hydrides as hydrogen storage materials is the slow sorption kinetics of hydrogen in the solid [8,9]. This can be partially alleviated by doping the magnesium hydride solids with a transition metal. While much is still unknown about which transition metal, and at which dopant concentration, is most effective, investigations have shown that titanium and similar early transition metal-doped magnesium hydride materials show better sorption kinetics compared to other metal dopants [10,11]. In addition, Mg_7TiH_x solids are stable and have been prepared that release hydrogen at lower temperature requirements than both pure magnesium hydrides and titanium hydrides [12]. Likewise, mixed magnesium-scandium materials have demonstrated good hydrogen uptake and storage capacity [13]. Hence, these transition metals are two of the more promising candidates to improve the hydrogen sorption kinetics in magnesium hydride solid materials. Thus, research is actively being explored on scandium- and titanium-doped magnesium and magnesium hydride clusters for hydrogen storage [14–21].

In order to understand the detailed binding characteristics and hydrogen saturation limits of small cluster systems, we previously studied the structures and properties of various $MgScH_n$ and $MgTiH_n$ clusters using standard density functional theory (DFT) methods [22,23]. Clusters, such as these, are frequently used as models for larger bulk materials and real-world applications [24]. Advances in, and access to, high-performance computing (hpc) technologies now allow for both of these $MgMH_n$ systems (M = Sc, Ti) to be investigated at a higher level of theory, allowing for a more accurate and detailed comparison of the two transition metal dopants and their role in improving hydrogen sorption kinetics. We report the results from these investigations here with the main goals to (1) investigate the precise cluster structures of $MgScH_n$ and $MgTiH_n$ clusters using a double-hybrid DFT method for the first time, (2) determine discrepancies and similarities in the assigned ground state structures at this new higher level of theory, and (3) re-analyze cluster stability, and other electronic properties, determining which sizes are the most stable for each dopant metal. To our knowledge, this is the first report using a double-hybrid DFT method to study transition metal–magnesium-hydrogen cluster systems, and this study additionally provides a novel benchmark study for these advanced computational chemistry methods for use in exploring transition metal-doped magnesium hydride materials.

2. Theoretical Methods

Initial cluster structures that were considered were taken from low-energy isomers reported previously, were created by hand, or were generated by using the unbiased global optimization ABCluster 2.1 program [22,23,25–27]. We have previously demonstrated the need to use a global optimization procedure, rather than solely relying on prior experiences, to locate the correct global minima structures of clusters [28]. All candidate isomers were then stringently optimized using the DSDPBEP86 double-hybrid DFT method with Grimme's D3BJ dispersion corrections coupled with the large 6-311++G(3df,3pd) basis set for all atoms [29–31]. This method was chosen for several reasons. For example, this double-hybrid method has been shown to reproduce theoretical predictions nearing the coupled cluster level of theory, while taking the computational time similar to Møller–Plesset levels [29]. It has also accurately reproduced experimental results for a variety of systems [32,33], and logically expands upon the theoretical levels previously employed for these cluster systems (both in terms of method and basis sets). To illustrate the addi-

tional computational demand of the higher double-hybrid method employed here (i.e., DSDPBEP86/6-311++G(3df,3pd)), optimization and vibrational frequency calculations on small MgTiH clusters took on average over 11 times longer to complete than at the lower level B3PW91/6-311++G(d,p) level employed previously when both had otherwise identical input files. Although double-hybrid DFT methods have higher computational costs compared to standard and hybrid DFT techniques, they (and DSD-type double-hybrids in particular) approach the accuracy of wavefunction methods in terms of predicting energetics, vibrational frequencies, reactions, and other properties [29,34]. The Gaussian 16, revision C.01, program package was used for all calculations [35]. Vibrational frequencies were calculated to ensure true minima structures were located with no imaginary frequencies, and all reported energy values include zero-point energy corrections. Although various spin states were tested, all reported global minima adopt the lowest possible spin state (i.e., either with spin multiplicity 2s + 1 = 1 or 2). To further understand the cluster's electronic properties, natural bond orbital analysis was performed using the NBO 7 program [36]. Calculations were performed on the Expanse hpc cluster housed at the San Diego Supercomputing Center (SDSC) through the NSF-ACCESS program [37,38]. The optimized structures and various properties were visualized using the GaussView 6 program [39]. The xyz coordinates for all ground state structures reported here are provided in the Supporting Information for this article.

3. Results and Discussion

3.1. Geometric Structure Determination and Growth Mechansim

3.1.1. $MgMH_n$ (n = 1–6)—Formation of $Mg(\mu\text{-}H)_3M$ Subunits

The determined ground state structures for all $MgMH_n$ clusters (M = Sc, Ti; n = 1–18) are shown in Figure 1. The triatomic MgScH and MgTiH species form small triangular clusters with the hydrogen atom bridging each transition metal–magnesium bond. These smallest-sized clusters are similar to those predicted previously at the B3PW91/6-311++G(d,p) level of theory [23]. For comparison and reference, the optimized Mg-H, Mg-Sc, and Sc-H distances in MgScH are predicted to be 2.458 Å, 3.205 Å, and 1.794 Å here at the DSDPBEP86/6-311++G(3df,3pd) level, whereas they are 2.423 Å, 3.165 Å, and 1.787 Å at the lower B3PW91/6-311++G(d,p) level. For the small analogous titanium species, the optimized Mg-H, Mg-Ti, and Ti-H distances are predicted to be 2.222 Å, 2.828 Å, and 1.841 Å here at the DSDPBEP86/6-311++G(3df,3pd) level, but were previously 2.130 Å, 2.772 Å, and 1.807 Å at the lower B3PW91/6-311++G(d,p) level of theory. Hence, the optimized distances with the double-hybrid DSDPBEP86 methods are slightly longer than those at the previously reported B3PW91 hybrid DFT level for $MgMH_1$ species. The Mg-M length using the larger double-hybrid method as the cluster size grows with additional hydrogen atoms is depicted in Figure 2. We note that while the Mg-M distance is larger at the DSDPBEP86 level for some smaller-sized $MgMH_n$ clusters than the B3PW91 method (such as for $MgMH_1$), the Mg-M distance is almost exclusively shorter at the DSDPBEP86 level for larger clusters. That is, the Mg-M distance is, with few exceptions, shorter in $MgMH_n$ clusters using the double-hybrid DFT method when $n > 6$ for both transition metals.

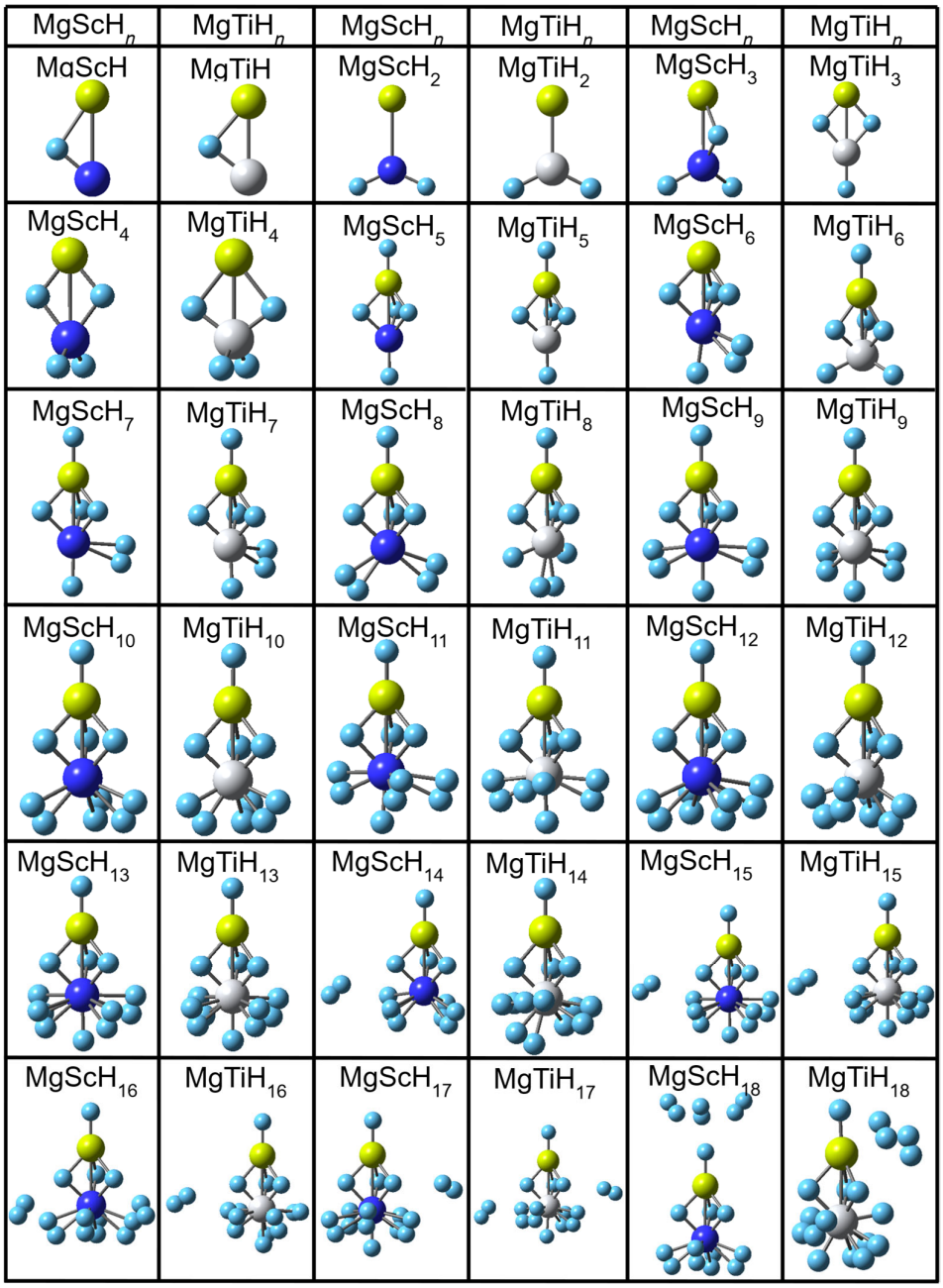


Figure 1. Located ground state structures of $MgMH_n$ (n = 1–18; M = Sc, Ti) at the DSDPBEP86/6-311++G(3df,3pd) level of theory. Magnesium atoms are colored yellow, scandium atoms are dark blue, titanium atoms are gray, and smaller hydrogen atoms are light blue in each structure. Coordinates for each structure are provided in the Supporting Information.

$MgScH_2$ and $MgTiH_2$ are both related structures with the two hydrogen atoms binding to the transition metal center as individual H atoms, which is a similar structure to that reported previously with the lower B3PW91 method [23]. However, for $MgMH_3$, different ground state structures are located for $MgScH_3$ and $MgTiH_3$. Hence, reported for the first time, this is the smallest size determined with a metal dependence on hydrogen binding to $MgMH_n$ clusters. $MgScH_3$ contains two hydrogen atoms bound to Sc with one additional hydrogen atom bridging both scandium and magnesium (i.e., bridging the Sc-Mg bond). $MgTiH_3$ contains one hydrogen atom bound to Ti with two additional hydrogen atoms bridging Ti-Mg. Note that neither of these structures is the same as that found for $MgTiH_3$ at the B3PW91/6-311++G(d,p) level, which contained three bridge-bound hydrogen atoms.

At the DSDPBEP86/6-311++G(3df,3pd) level, this $MgTiH_3$ isomer is found to lie 9.2 kJ/mol higher in energy than the lowest energy structure shown in Figure 1. Hence, this is also the smallest-sized cluster where a new ground state isomer is located at this higher double-hybrid level of theory, demonstrating the importance of higher-level theoretical predictions of atomic clusters.

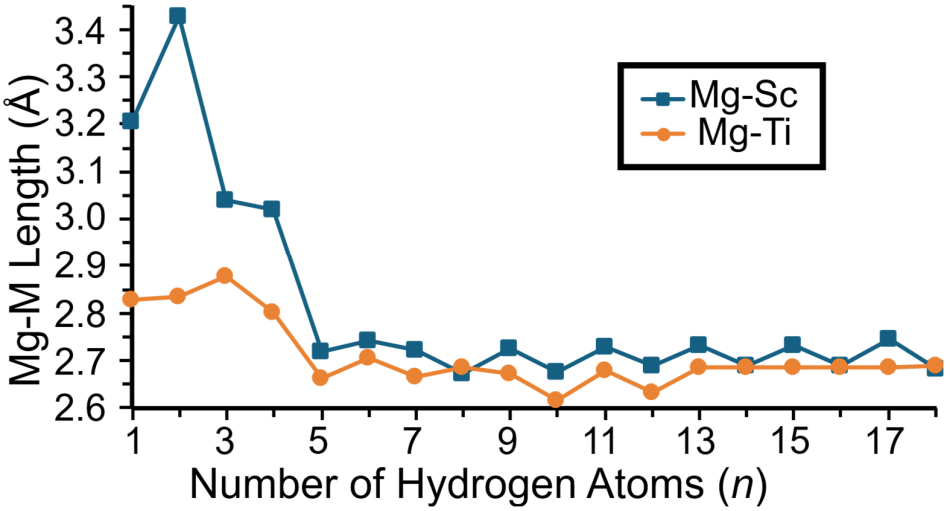


Figure 2. Distance between magnesium and scandium (blue squares) or magnesium and titanium (orange circles) versus the number of hydrogen atoms in $MgMH_n$ clusters (n = 1–18; M = Sc, Ti).

$MgMH_4$ and $MgMH_5$ ground state structures are similar for both scandium and titanium transition metals, and are similar to the lowest energy geometries found previously for $MgTiH_n$ [23]. For $MgMH_5$, we note that this is the smallest size with a hydrogen atom bound solely on magnesium. This is also the size where an H-Mg(μ-H)$_3$M unit first appears for both scandium and titanium. This unit will be prevalent and discussed further in the next section for larger clusters. We also note in Figure 2 that the Mg-M distance has decreased in $MgMH_5$ for both scandium- and titanium-containing clusters, and that the distance remains small for larger sizes. Hence, this Mg(μ-H)$_3$M unit (which is present in all larger sizes) aids in decreasing the Mg-M bond distance. $MgMH_6$ again shows a difference between the two transition metals. Both $MgScH_6$ and $MgTiH_6$ have three bridge-bound hydrogen atoms and form a Mg(μ-H)$_3$M subunit. However, $MgScH_6$ contains three additional hydrogen atoms bound on the Sc center (one as a hydrogen atom, and two hydrogen atoms as molecular H_2), whereas $MgTiH_6$ contains only two hydrogens on the Ti center (as individual hydrogen atoms) with the last hydrogen atom bound on Mg. While this is a uniquely different structure for $MgScH_6$ than reported previously with the lower B3PW91 method, it is the same structure found previously for $MgTiH_6$ [22,23].

3.1.2. $MgMH_n$ (n = 7–12)—Continued Hydrogen Aggregation on Transition Metal Centers

The located ground state structures for $MgScH_7$ and $MgTiH_7$ both contain H-Mg(μ-H)$_3$M units, with three additional hydrogen atoms bound to the transition metal center. In both cases, the additional three hydrogens are coordinated as an H_2 molecule and a separate H atom to the transition metal center (Figure 1). This is similar to that predicted at the B3PW91 level of theory [22,23]. For $MgMH_8$, a difference is again noted between ground state structures with Sc and Ti transition metals. Both contain the H-Mg(μ-H)$_3$M unit, with four additional hydrogens bound to the transition metal atom. However, these four hydrogen atoms bind as two H_2 molecules for Sc, but as a single H_2 molecule and two separate H atoms for Ti, which is similar to that predicted previously at the B3PW91 level of theory [22,23]. Hence, the difference seems indeed to be due to the different transition

metals, and is method independent (see additional details in the $MgScH_n$ and $MgTiH_n$ comparison section below).

For $MgMH_9$—$MgMH_{12}$, hydrogen atoms continue to aggregate on the Sc and Ti metal centers. For each $MgMH_n$ with an odd number of hydrogen atoms, there is an H-Mg(μ-H)$_3$M unit with an additional single H atom bound to the transition metal and the remaining hydrogens bound as H_2 units on the transition metal center. For each $MgMH_n$ with an even number of hydrogen atoms, there is an H-Mg(μ-H)$_3$M unit with all remaining hydrogens bound as H_2 units on the transition metal (i.e., there is not a lone H atom attached to the metal as there is for species containing an odd number of hydrogen atoms). The structures are similar to each other for both transition metals, are similar to the structures predicted at the B3PW91 level of theory [22,23], and do not need additional comment here.

3.1.3. $MgMH_n$ (n = 13–18)—Hydrogen Saturation and Dissociation

The structures for $MgScH_{13}$ and $MgTiH_{13}$ continue to build upon the smaller clusters reported in the previous section, and have additional hydrogen atoms coordinating to each transition metal center. For each metal, the lowest energy isomer located at the DSDPBEP86/6-311++G(3df,3pd) method shown in Figure 1 is related to that reported previously at the B3PW91/6-311++G(d,p) level [22,23], with a few small differences described below. The harmonic H_2 stretching frequencies for diatomic hydrogen units in these clusters are provided in Table S2 of the Supporting Information, and show a weakening of the H_2 bond, confirming all of the molecular hydrogens are interacting in the cluster at this size.

For $MgScH_{14}$, our double-hybrid calculations predict a ground state isomer with a dissociated H_2 molecule. This structure can be seen as $MgScH_{12}$ with an additional dissociated H_2. The H-H bond lengths for the five H_2 units in $MgScH_{14}$ are predicted to be 0.7746 Å, 0.7724 Å, 0.7721 Å, 0.7599 Å, and 0.7433 Å, with the last belonging to what we refer to as the dissociated H_2. As our calculations predict the bond length in free H_2 to be 0.7417 Å, four of the five H_2 molecules in $MgScH_{14}$ show considerably more bond weakening due to the interaction in the cluster than the dissociated H_2. Table S2 in the Supporting Information also shows that four of the five H_2 stretching frequencies in $MgScH_{14}$ are at considerably lower frequencies than free H_2, whereas one H_2 frequency (belonging to the dissociated H_2) is only red-shifted by <35 cm^{-1} from that predicted for free H_2. Hence, for species with scandium, $MgScH_{13}$ is saturated with hydrogen and dissociation begins at the next larger size (i.e., for $MgScH_{14}$). This is similar to our previous report using a lower level of theory [22]. However, a different report has also indicated that $MgScH_{14}$ contained all hydrogen atoms bound to Mg or Sc, and these two investigations conflicted on the saturation size where dissociation occurs in $MgScH_n$ clusters [22,25]. We previously reported this species with all bound hydrogens to be 8.6 kJ/mol higher in energy at the B3PW91/6-311++G(d,p) level, and 4.0 kJ/mol higher in energy at the MP2/6-311++G(3df,3pd) level [22]. Here, at the DSDPBEP86/6-311++G(3df,3pd) level, this isomer without a dissociated H_2 is only 0.7 kJ/mol higher in energy than the ground state isomer reported in Figure 1. Regardless, this now demonstrates that even at this higher-level double-hybrid method, hydrogen is predicted to dissociate already for $MgScH_{14}$. However, the presence of isomers containing a dissociated hydrogen molecule, and an isomer with no dissociated H_2, lying close in energy, further indicates that this is a transitional size in the growth of $MgScH_n$ clusters. It is interesting to note that we also find a low-energy isomer with H_2 dissociated, but coordinated to the H-Mg-Sc backbone, which lies only 0.6 kJ/mol higher in energy than the ground state in Figure 1 at this DSDPBEP86/6-311++G(3df,3pd) level of theory. This isomer has been reported as 1.8 kJ/mol and

0.5 kJ/mol higher in energy at the B3PW91/6-311++G(d,p) and MP2/6-311++G(3df,3pd) levels, respectively [22], and has been proposed as an isomer of particular interest in a possible route for H_2 dissociation in transition metal-doped magnesium hydride clusters and materials. That is, it has been suggested that H_2 dissociation occurs by coordinating to the anionic hydride in the H-Mg-M backbone of the cluster through species resembling this intermediate. The presence of this low-lying isomer here, with a large negatively charged hydride (−0.504 Mulliken charge, −0.528 APT charge, −0.696 NBO charge) further supports this possible dissociation pathway. Regardless, our main point here is that $MgScH_{14}$ contains a dissociated H_2 molecule.

The ground state isomer for $MgTiH_{14}$ at this level (Figure 1) contains all hydrogen atoms bound to the metal core, and hydrogen has not dissociated yet for the titanium analog at this size. The H-H bond distances are predicted to be 0.8553 Å, 0.8152 Å, 0.8152 Å, 0.7885 Å, and 0.7885 Å in $MgTiH_{14}$. These are all longer than the predicted 0.7417 Å distance in free H_2. Note also the large red shift in H_2 stretching frequencies (provided in Table S2 in the Supporting Information) for the diatomic hydrogen units in this cluster. Hence, all of the H_2 molecules show some interaction within the cluster, weakening the H-H bond, and we state that no H_2 is dissociated in the $MgTiH_{14}$ cluster. This is in agreement with the lower B3PW91/6-311++G(d,p) results [23], and confirms that the structures for $MgMH_{14}$ (M = Sc, Ti), and hence the saturation limit, are different depending on the transition metal dopant.

The ground state structures of $MgMH_{15}$ (M = Sc, Ti) are also shown in Figure 1. $MgScH_{15}$ builds upon $MgScH_{14}$ by adding a single H atom to the Sc center and still having a dissociated H_2 molecule along the cluster's side. For $MgTiH_{15}$, the ground state structure possesses a single dissociated H_2 unit on an analogous $MgTiH_{13}$ structure. Here, the five H-H bond lengths in $MgTiH_{15}$ are predicted to be 0.7794 Å, 0.7790 Å, 0.7687 Å, 0.7683 Å, and 0.7427 Å. The last (smallest) H-H length, which is close to the 0.7417 Å distance predicted in free H_2, is the length associated with the hydrogen molecule we are referring to as dissociated. Hence, $MgTiH_{15}$ is the first size cluster with titanium to have a dissociated H_2 molecule, and $MgTiH_n$ clusters are saturated with hydrogen at $MgTiH_{14}$. It is interesting to note that the saturation limit in these clusters is indeed transition metal dependent (i.e., $MgScH_{13}$ and $MgTiH_{14}$ are the saturation limits for $MgScH_n$ and $MgTiH_n$ clusters, respectively). It is also worth noting here that a prior investigation using the B3PW91 method predicted $MgScH_{15}$ to be the saturation limit [25], a claim we disputed using the same theoretical method [22]. This study, using a high DSDPBEP86 level of theory, further validates these saturation limits, and the structures reported here are similar to those determined previously at the B3PW91/6-311++G(d,p) level [22,23].

For $MgMH_{16}$-$MgMH_{18}$, the ground state structures are determined, which continue to resemble saturated $MgScH_n$ (n = 12, 13) and $MgTiH_n$ (n = 13, 14) with additional H_2 molecules, with small deviations denoted below for each size. These structures are, in general, similar to those reported previously at lower levels of theory [22,23]. However, it is interesting to note that the dissociated H_2 molecules are at different positions around the core cluster compared to previous predictions. This is not entirely unexpected, as the dissociated H_2 molecules are only weakly interacting, and we have already shown that the dissociated H_2 molecule is predicted to be at different positions with the MP2 method for $MgScH_{17}$ and $MgScH_{18}$ compared to that predicted at the B3PW91/6-311++G(d,p) level of theory (and the DSDPBEP86 method used here contains some MP2 character). Hence, it appears that the position of weakly bound dissociated H_2 may be more dependent on the method employed, and this study at the DSDPBEP86/6-311++G(3df,3pd) level provides a new higher-level reference for the position and interaction of the H_2 molecule while dissociating from scandium- and titanium-doped magnesium hydride materials. The

predicted lowest energy structures in this size range are also depicted in Figure 1, and the coordinates are provided in the Supporting Information. For $MgScH_{18}$ where the three dissociated H_2 molecules coordinate to the anionic hydride along the Sc-Mg-H backbone, the hydride in the cluster is predicted to have a large negative charge (−0.513 Mulliken charge, −0.541 APT charge, −0.689 NBO charge). This again provides support for a possible route for H_2 dissociation from $MgMH_n$ clusters, with each molecular hydrogen being stabilized by coordinating to anionic hydrides in the cluster. $MgTiH_{18}$ is a unique cluster in this section which merits additional comments here. For the ten hydrogen atoms bound to the Ti center in $MgTiH_{18}$, eight of them are bound as (four) H_2 molecules, and the remaining two are bound as individual atoms. This cluster is uniquely different compared to others in this size range in that other sizes have all hydrogens bound as H_2 molecules (for even n), or contain only one single H atom bound to the transition metal (for odd n). That is, $MgTiH_{18}$ is the only cluster in this size range to have multiple single H atoms bound to the transition metal. All attempts to find a $MgTiH_{18}$ isomer with five H_2 molecules bound to Ti ended with isomers lying at least 10.4 kJ/mol higher in energy than the ground state structure depicted in Figure 1. It is also interesting to note that in this larger size range, for all sizes of $MgMH_n$ ($n > 13$), differences in the ground state structures are noted between species containing the Sc and Ti dopant atoms. Only for smaller sizes (i.e., $n \leq 13$) are similar structures noted for most, but not all, sizes as described in more detail later in the section dedicated to comparing the two transition metals.

3.2. Cluster Stability, Energetics, and Electronic Properties

The relative stabilities of each cluster size can be analyzed in several ways. Here, we first calculate a binding energy (fragmentation energy) for each ground state species by Equation (1), which compares the energy of each cluster with the sum of the energy of the individual H, Mg, and M (M = Sc or Ti) atoms making up the cluster.

$$E_{bind}(n) = \frac{E_{Mg} + E_M + nE_H - E_{MgMH_n}}{n+2}; M = Sc, Ti \quad (1)$$

Equation (1) is normalized for the increasing size of the cluster by dividing by the total number of atoms (i.e., the number of hydrogen atoms plus 2). It is standard to calculate the binding energy this way in terms of individual atoms and to normalize it by the total number of atoms [14,15,18,19,22,23,25,28,40,41], but we have also provided it in different ways (see further discussion later in this paragraph and in Table S1 of the Supporting Information). A plot of the binding energy calculated in Equation (1) as a function of cluster size for each metal is shown in Figure 3, and a few things merit comment. First, all binding energies are positive, indicating that each cluster is more stable than the individual atoms. Second, an oscillation is observed when there is an odd or even number of hydrogen atoms present in the cluster. We have noted previously that $MgMH_n$ clusters with an odd number of hydrogens tend to have a larger binding energy and be more stable than their counterparts with an even number of hydrogen atoms [23]. Clusters with an odd number of hydrogens present have new M-H interactions (rather than M-(H_2) interactions) occurring, which helps explain this observation. For example, in looking at the structures in Figure 1 for the middle sizes presented in the insert in Figure 3 (i.e., $MgMH_n$; n = 9–14), we see that those structures for both transition metals that contain an odd number of hydrogen atoms contain a lone M-H bond. That is, aside from the H-Mg(μ-H)$_3$M unit present in all of these clusters, $MgMH_9$, $MgMH_{11}$, and $MgMH_{13}$ contain an additional two, three and four H_2 molecules, respectively, and a single H atom bound to the transition metal. Clusters with an even number of hydrogen atoms (i.e., $MgMH_{10}$, $MgMH_{12}$, and $MgMH_{14}$) contain an additional two, three and four H_2 molecules, respectively, without any additional H

atoms bound to the transition metal center. It is this fundamental difference in the presence of M-H vs. M-(H_2) groups that gives rise to this odd-even oscillation. The numerical values of the binding energies shown in Figure 3 are provided in Table S1 in the Supporting Information. This table also lists the binding energies calculated relative to H_2 molecules (rather than H atoms), as well as the calculated binding energies relative to a mixture of the H atoms and H_2 molecules that compose each individual cluster.

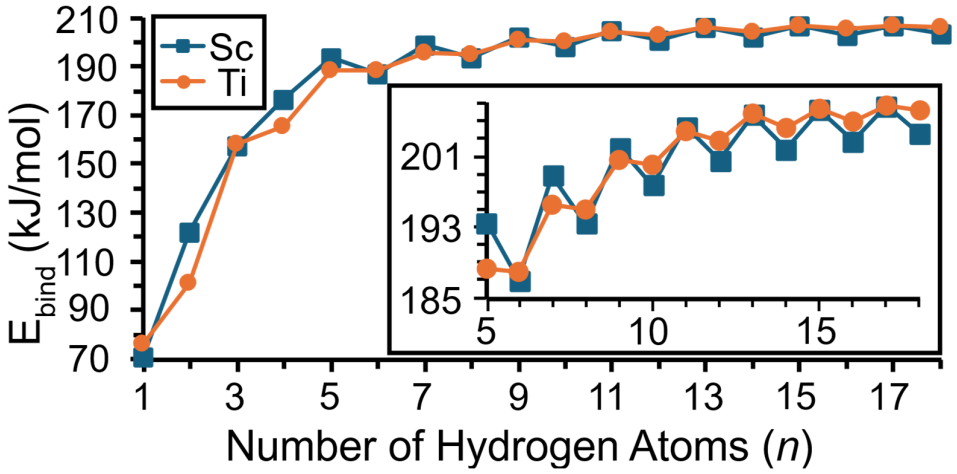


Figure 3. Plot of the binding energy (fragmentation energy) versus the number of hydrogen atoms in $MgMH_n$ clusters (n = 1–18), with the metal, M, being Sc (blue squares) and Ti (orange circles). The insert depicts an enlarged portion of the plot in the n = 5–18 size range.

A stabilization energy compares the energy of a given cluster size to related cluster sizes. We calculate a stabilization energy (E_{stab1}), as depicted in Equation (2), as twice the energy of the given cluster minus the energy of clusters containing one less and one more hydrogen atom.

$$E_{stab1}(n) = 2E_{MgMH_n} - E_{MgMH_{n-1}} - E_{MgMH_{n+1}}; M = Sc, Ti \quad (2)$$

A negative E_{stab1} indicates more stable clusters relative to their neighboring sizes. Given the odd/even oscillation observed in E_{bind}, a similar odd/even oscillation is expected for E_{stab1}. Hence, an E_{stab2} is also calculated by Equation (3), which compares the energy of a cluster with those of similar clusters also containing an odd or even number of hydrogen atoms. That is, E_{stab2} is calculated as twice the energy of a cluster minus the energy of clusters containing two fewer and two more hydrogen atoms.

$$E_{stab2}(n) = 2E_{MgMH_n} - E_{MgMH_{n-2}} - E_{MgMH_{n+2}}; M = Sc, Ti \quad (3)$$

E_{stab1} and E_{stab2} are plotted in Figure 4 for both the Sc and Ti metals in $MgMH_n$ clusters. In looking at these plots, a larger negative number suggests a cluster size that is more stable than others for both E_{stab1} and E_{stab2}. We note that smaller clusters often have larger negative stabilization energies. This has been noted previously and is due, in part, to the dramatic change in structure made sometimes by adding a single hydrogen in these small clusters. Perhaps more important are the observed clusters of enhanced stability once the H-Mg(μ-H)$_3$M unit is formed and remains (i.e., for $MgMH_n$; $n \geq 7$ clusters), and the cluster size range approaching the saturation limit. In this region, the energies are more comparable, but local minima appear present for $MgScH_{12}$ and $MgTiH_{10}$ (for species containing an even number of hydrogen atoms), and for $MgTiH_{13}$ (for species containing an odd number of hydrogen atoms). This particular size region for E_{stab2} is discussed in

more detail for each transition metal in the next section, which compares both $MgScH_n$ and $MgTiH_n$ clusters.

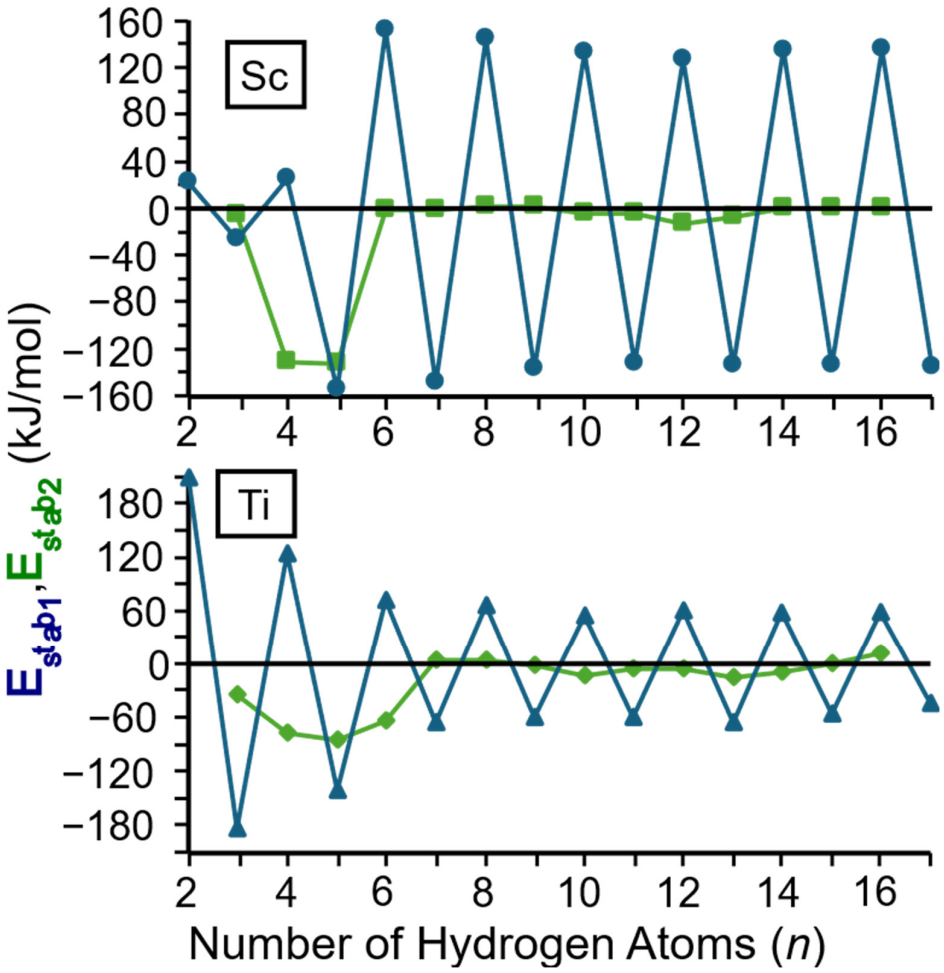


Figure 4. Plot of the first and second stabilization energies versus the number of hydrogen atoms in $MgMH_n$ clusters (n = 2–17), with the metal, M, being Sc (**top**) and Ti (**bottom**). The first stabilization energy is shown in blue (circles for Sc, triangles for Ti), and the second stabilization energy is plotted in green (squares for Sc, diamonds for Ti).

While these clusters are clearly stable, we note again that a major importance of cluster studies is to provide detailed studies on smaller systems that may be extended to, and provide insight about, larger bulk materials. While the dissociated H_2 molecule(s) in larger clusters here are only slightly perturbed from free H_2 (for example, the harmonic frequencies listed in Table S2 in the Supporting Information are only slightly perturbed in the dissociated H_2 units), the bound clusters are predicted to be stable and likely could be formed in at least gas-phase experiments. The strength of the interaction of molecular hydrogen with the cluster, which has been discussed in terms of H_2 bond elongation and stretching frequency red shifts, is related to dehydrogenation enthalpy and desorption temperature properties. The binding energy (fragmentation energy) in terms of fragmenting H_2 molecules (rather than H atoms) is further analyzed in Table S1 in the Supporting Information.

The predicted partial charges (i.e., Mulliken and Natural charges) and Natural Electron Configurations (NECs) for each magnesium and transition metal atom in $MgMH_n$ clusters are provided in Table 1 (for n = 1–10) and Table 2 (for n = 11–18). In looking at the charges, we notice first that Natural charges are typically, with a few exceptions, predicted to be larger in magnitude than Mulliken charges for Mg, Sc, and Ti. We also notice that the

sign of both the Natural and Mulliken partial charges for all three metals is the same for all sizes. Magnesium and scandium atoms are always predicted to be partially positively charged. Titanium is predicted to be partially positively charged in $MgTiH_n$ clusters for n = 1–11, and then is predicted by both charge schemes to be partially negatively charged for $n \geq 12$. This is uniquely different from a previous study at the lower B3PW91 level of theory where Ti was predicted to have a partial negative Mulliken charge in $MgTiH_{10}$ and $MgTiH_{11}$ [23]. We also note that Sc in $MgScH_n$ (n = 12–20) has previously been predicted to have a negative Natural charge at a lower B3PW91 level of theory [25], whereas a more recent investigation contradicted this and suggested a small positive partial Natural charge on Sc in this size range [22]. This investigation at the higher double-hybrid DSDPBEP86 level further validates a prediction of a positive Natural charge on Sc in all cluster sizes.

In looking at the Natural Electron Configurations in Tables 1 and 2, it is noted that the partial positive charges in Mg primarily arise from a loss of electron density in the 3s atomic orbital. The partial charges in Sc and Ti both come about largely from a loss of electron density in the 4s atomic orbital, and a gain of electron density in the 3d atomic orbital. It is interesting to note that the only exception to this for the species studied here is for small $MgScH_n$ ($n \leq 5$), where Sc loses electron density from both the 4s and 3d atomic orbitals. Comparing the NECs here to those predicted previously at the lower B3PW91 level, a main difference is in the 3d atomic orbital of the transition metal. While the metal is still predicted to accept electron density in the 3d atomic orbital at the DSDPBEP86 level, it is predicted to accept less electron density than at the lower B3PW91 level [22,23]. The full predicted NECs for Mg, Sc, and Ti for all sizes studied here using the DSDPBEP86 method are provided in Tables 1 and 2. The highest occupied molecular orbitals (HOMOs) or singly occupied molecular orbitals (SOMOs) for $MgMH_n$ (M = Sc, Ti; n = 13–15) at the transitional size region where dissociation begins to occur are provided as Figure S1 in the Supporting Information. They show that these frontier orbitals are comprised primarily of hydrogen s and transition metal d atomic orbitals. We also note that the frontier orbitals of $MgMH_{13}$ and $MgMH_{15}$ are quite similar, showing that the dissociated molecular hydrogen does not play a significant role in the MO. That is, $MgMH_{15}$, which adopts a similar structure to $MgMH_{13}$ with an additional dissociated H_2 as described above, has a similar HOMO to $MgMH_{13}$ (as well as a similar NEC as shown in Table 2).

3.3. $MgScH_n$ and $MgTiH_n$ Comparison

Comparing the geometries of $MgScH_n$ and $MgTiH_n$ (n = 1–18) in Figure 1, we first note similar geometries regardless of the transition metal for n = 1, 2, 4, 5, 7, 9, 10, 11, 12, 13, and 15. $MgMH_3$ is the first size that shows a transition metal dependence, with $MgTiH_3$ preferring a structure with two hydrogen atoms bridging Ti-Mg, and $MgScH_3$ preferring a structure with only one hydrogen atom bridging Sc-Mg. As both metals prefer a structure with no M-Mg bridging hydrogen atoms in $MgMH_2$, and both metals prefer a structure with two M-Mg bridging hydrogen atoms in $MgMH_4$, $MgMH_3$ is evidently a transitional size in the preferred hydrogen location in these clusters. $MgMH_6$ (M = Sc, Ti) each have a $Mg(\mu\text{-}H)_3M$ unit, with Sc preferring the three additional hydrogen atoms on Sc, whereas Ti prefers a structure with two hydrogen atoms on Ti, and the remaining hydrogen atom bound solely on magnesium. The $MgMH_8$ (M = Sc, Ti) clusters have nearly similar geometries with four hydrogen atoms bound solely on the transition metal. However, $MgScH_8$ adopts a structure where these four hydrogens are present as H_2 molecules, whereas $MgTiH_8$ adopts a structure with one H_2 molecule and two individual H atoms.

Table 1. Natural Electron Configuration (NEC), Mulliken charges, and Natural charges for each metal atom in $MgMH_n$ (M = Sc, Ti; n = 1–10) clusters.

H Atoms (n)	M	NEC	Mulliken Charge (Mg/M)	Natural Charge (Mg/M)
1	Sc	Mg:$3s^{1.82}$ $3p^{0.04}$ $4s^{0.01}$ $3d^{0.01}$	0.207/0.106	0.130/0.457
		Sc:$4s^{1.70}$ $3d^{0.71}$ $4p^{0.10}$ $5s^{0.01}$ $4d^{0.02}$		
	Ti	Mg:$3s^{1.62}$ $3p^{0.06}$ $3d^{0.01}$	0.213/0.110	0.307/0.442
		Ti:$4s^{1.13}$ $3d^{2.33}$ $4p^{0.08}$ $4d^{0.02}$		
2	Sc	Mg:$3s^{1.81}$ $3p^{0.09}$	0.064/0.701	0.094/1.150
		Sc:$4s^{0.91}$ $3d^{0.81}$ $4p^{0.11}$ $4d^{0.01}$		
	Ti	Mg:$3s^{1.68}$ $3p^{0.05}$ $3d^{0.01}$	0.213/0.493	0.263/0.918
		Ti:$4s^{0.50}$ $3d^{2.42}$ $4p^{0.13}$ $4d^{0.02}$ $4f^{0.01}$		
3	Sc	Mg:$3s^{1.67}$ $3p^{0.04}$ $3d^{0.01}$	0.279/0.851	0.276/1.592
		Sc:$4s^{0.47}$ $3d^{0.82}$ $4p^{0.09}$ $4d^{0.02}$		
	Ti	Mg:$3s^{1.06}$ $3p^{0.07}$ $3d^{0.01}$	0.513/0.474	0.854/1.249
		Ti:$4s^{0.36}$ $3d^{2.35}$ $4p^{0.01}$ $4d^{0.03}$		
4	Sc	Mg:$3s^{1.03}$ $3p^{0.07}$ $3d^{0.01}$	0.527/0.975	0.893/1.691
		Sc:$4s^{0.47}$ $3d^{0.78}$ $4p^{0.04}$ $4d^{0.01}$		
	Ti	Mg:$3s^{1.31}$ $3p^{0.03}$ $4s^{0.01}$	0.559/0.684	0.639/1.094
		Ti:$4s^{0.61}$ $3d^{2.19}$ $4p^{0.07}$ $4d^{0.03}$ $4f^{0.01}$		
5	Sc	Mg:$3s^{0.48}$ $3p^{0.02}$	0.879/0.784	1.484/1.696
		Sc:$4s^{0.37}$ $3d^{0.88}$ $4p^{0.03}$ $4d^{0.02}$		
	Ti	Mg:$3s^{0.48}$ $3p^{0.02}$	0.909/0.511	1.485/1.387
		Ti:$4s^{0.38}$ $3d^{2.16}$ $4p^{0.03}$ $4d^{0.03}$ $4f^{0.01}$		
6	Sc	Mg:$3s^{1.00}$ $3p^{0.05}$ $3d^{0.01}$	0.490/0.770	0.927/1.460
		Sc:$4s^{0.41}$ $3d^{1.08}$ $4p^{0.02}$ $4d^{0.02}$		
	Ti	Mg:$3s^{0.46}$ $3p^{0.02}$	0.731/0.605	1.502/1.095
		Ti:$4s^{0.45}$ $3d^{2.37}$ $4p^{0.04}$ $4d^{0.03}$ $4f^{0.01}$		
7	Sc	Mg:$3s^{0.48}$ $3p^{0.02}$	0.819/0.700	1.491/1.550
		Sc:$4s^{0.37}$ $3d^{1.03}$ $4p^{0.02}$ $4d^{0.02}$		
	Ti	Mg:$3s^{0.47}$ $3p^{0.02}$	0.839/0.423	1.495/1.125
		Ti:$4s^{0.38}$ $3d^{2.42}$ $4p^{0.02}$ $4d^{0.05}$ $4f^{0.01}$		
8	Sc	Mg:$3s^{0.47}$ $3p^{0.02}$	0.728/0.663	1.499/1.067
		Sc:$4s^{0.27}$ $3d^{1.62}$ $4p^{0.02}$ $4d^{0.02}$		
	Ti	Mg:$3s^{0.45}$ $3p^{0.02}$	0.830/0.337	1.514/0.685
		Ti:$4s^{0.40}$ $3d^{2.83}$ $4p^{0.02}$ $4d^{0.05}$ $4f^{0.01}$		
9	Sc	Mg:$3s^{0.47}$ $3p^{0.02}$	0.784/0.673	1.499/1.349
		Sc:$4s^{0.36}$ $3d^{1.24}$ $4p^{0.02}$ $4d^{0.02}$		
	Ti	Mg:$3s^{0.47}$ $3p^{0.02}$ $3d^{0.01}$	0.770/0.229	1.502/0.876
		Ti:$4s^{0.40}$ $3d^{2.64}$ $4p^{0.02}$ $4d^{0.06}$ $4f^{0.01}$		
10	Sc	Mg:$3s^{0.46}$ $3p^{0.02}$	0.758/0.452	1.507/0.839
		Sc:$4s^{0.28}$ $3d^{1.84}$ $4p^{0.01}$ $4d^{0.02}$ $4f^{0.01}$		
	Ti	Mg:$3s^{0.46}$ $3p^{0.02}$	0.800/0.020	1.513/0.188
		Ti:$4s^{0.36}$ $3d^{3.38}$ $4p^{0.01}$ $4d^{0.04}$ $4f^{0.01}$		

Table 2. Natural Electron Configuration (NEC), Mulliken charges, and Natural charges for each metal atom in $MgMH_n$ (M = Sc, Ti; n = 11–18) clusters.

H Atoms (n)	M	NEC	Mulliken Charge (Mg/M)	Natural Charge (Mg/M)
11	Sc	Mg:$3s^{0.46}$ $3p^{0.02}$	0.739/0.603	1.507/1.124
		Sc:$4s^{0.37}$ $3d^{1.47}$ $4p^{0.01}$ $4d^{0.02}$ $4f^{0.01}$		
	Ti	Mg:$3s^{0.46}$ $3p^{0.02}$ $3d^{0.01}$	0.717/0.084	1.510/0.426
		Ti:$4s^{0.38}$ $3d^{3.11}$ $4p^{0.01}$ $4d^{0.06}$ $4f^{0.01}$		
12	Sc	Mg:$3s^{0.46}$ $3p^{0.02}$ $3d^{0.01}$	0.616/0.501	1.510/0.652
		Sc:$4s^{0.29}$ $3d^{2.02}$ $4p^{0.01}$ $4d^{0.02}$ $4f^{0.01}$		
	Ti	Mg:$3s^{0.45}$ $3p^{0.02}$	0.706/−0.131	1.510/−0.151
		Ti:$4s^{0.36}$ $3d^{3.72}$ $4p^{0.01}$ $4d^{0.04}$ $4f^{0.01}$		
13	Sc	Mg:$3s^{0.45}$ $3p^{0.02}$	0.727/0.331	1.516/0.815
		Sc:$4s^{0.36}$ $3d^{1.79}$ $4p^{0.01}$ $4d^{0.02}$ $4f^{0.01}$		
	Ti	Mg:$3s^{0.44}$ $3p^{0.02}$ $3d^{0.01}$	0.622/−0.212	1.524/−0.075
		Ti:$4s^{0.37}$ $3d^{3.61}$ $4p^{0.01}$ $4d^{0.08}$ $4f^{0.01}$		
14	Sc	Mg:$3s^{0.46}$ $3p^{0.02}$ $3d^{0.01}$	0.582/0.499	1.510/0.650
		Sc:$4s^{0.29}$ $3d^{2.02}$ $4p^{0.01}$ $4d^{0.02}$ $4f^{0.01}$		
	Ti	Mg:$3s^{0.44}$ $3p^{0.02}$ $3d^{0.01}$	0.486/−0.298	1.530/−0.774
		Ti:$4s^{0.35}$ $3d^{4.35}$ $4p^{0.01}$ $4d^{0.04}$ $4f^{0.02}$		
15	Sc	Mg:$3s^{0.45}$ $3p^{0.02}$	0.681/0.366	1.516/0.813
		Sc:$4s^{0.36}$ $3d^{1.79}$ $4p^{0.01}$ $4d^{0.02}$ $4f^{0.01}$		
	Ti	Mg:$3s^{0.44}$ $3p^{0.02}$ $3d^{0.01}$	0.609/−0.190	1.525/−0.079
		Ti:$4s^{0.37}$ $3d^{3.61}$ $4p^{0.01}$ $4d^{0.08}$ $4f^{0.01}$		
16	Sc	Mg:$3s^{0.46}$ $3p^{0.02}$ $3d^{0.01}$	0.527/0.528	1.511/0.648
		Sc:$4s^{0.29}$ $3d^{2.02}$ $4p^{0.01}$ $4d^{0.02}$ $4f^{0.01}$		
	Ti	Mg:$3s^{0.44}$ $3p^{0.02}$ $3d^{0.01}$	0.445/−0.336	1.531/−0.777
		Ti:$4s^{0.35}$ $3d^{4.36}$ $4p^{0.01}$ $4d^{0.04}$ $4f^{0.02}$		
17	Sc	Mg:$3s^{0.44}$ $3p^{0.02}$ $3d^{0.01}$	0.563/0.390	1.523/0.484
		Sc:$4s^{0.36}$ $3d^{2.12}$ $4p^{0.01}$ $4d^{0.02}$ $4f^{0.01}$		
	Ti	Mg:$3s^{0.44}$ $3p^{0.02}$ $3d^{0.01}$	0.607/−0.253	1.525/−0.087
		Ti:$4s^{0.36}$ $3d^{3.62}$ $4p^{0.01}$ $4d^{0.07}$ $4f^{0.01}$		
18	Sc	Mg:$3s^{0.45}$ $3p^{0.02}$ $3d^{0.01}$	0.597/0.232	1.513/0.410
		Sc:$4s^{0.29}$ $3d^{2.26}$ $4p^{0.01}$ $4d^{0.02}$ $4f^{0.01}$		
	Ti	Mg:$3s^{0.43}$ $3p^{0.02}$ $3d^{0.01}$	0.632/−0.748	1.538/−0.737
		Ti:$4s^{0.41}$ $3d^{4.25}$ $4p^{0.01}$ $4d^{0.04}$ $4f^{0.02}$		

$MgMH_{14}$ (M = Sc, Ti) is the size with probably the most important structural difference. $MgScH_{14}$ prefers to have a dissociated H_2, whereas $MgTiH_{14}$ continues to have H_2 units bound to the metal centers. Hence, this difference sets the saturation limit for the small systems with different transition metals as $MgScH_{13}$ and $MgTiH_{14}$, which contain large 15.9% and 16.4% hydrogen by mass, respectively. Both $MgMH_{15}$ clusters (M = Sc, Ti) are similar with a dissociated H_2 molecule. $MgMH_n$ (n = 16–18, M = Sc, Ti) all change slightly depending on the transition metal, but often differ only in the position of the weakly interacting dissociated H_2 species. These positions are also often different from those predicted previously at the lower B3PW91 method, as described in the geometric structure determination section. Figure 2 shows the Mg-M distance for both scandium and titanium metals as the cluster grows in the number of hydrogen atoms. We have already noted that the distance is larger for smaller-sized clusters and remains fairly constant in $MgMH_n$ ($n \geq 5$). In comparing the effect of the transition metal, we note that Mg-Sc distances are longer than Mg-Ti distances in $MgMH_n$ for almost all clusters in the n = 1–18 size range.

We also note that for larger $MgMH_n$ species, where $n \geq 13$, the odd-even oscillation in Mg-M distances is more pronounced for scandium than it is for titanium. This was also noted at the B3PW91 level, that the Mg-Ti distance changes little for $MgTiH_n$ species where $n \geq 13$ [23].

Here, we also discuss the differences in the cluster stability (i.e., binding and relative energy) containing each transition metal in more depth. Figure 5 shows an enlargement of E_{stab2} (from Figure 4) for both metals in the $MgMH_7$–$MgMH_{16}$ size range. We notice that the most stable $MgScH_n$ clusters predicted by E_{stab2}, seen as local minima in the plots in Figure 5, are $MgScH_{12}$ and $MgScH_{13}$ for clusters with an even and odd number of hydrogens, respectively. For $MgTiH_n$, $MgTiH_{13}$ and $MgTiH_{10}$ are the most stable clusters with an odd and even number of hydrogens with respect to E_{stab2}, respectively. Although it is clearer here in Figure 5, these sizes are also evident as the most stable species containing an odd and even number of hydrogen atoms in inspecting E_{stab1} in Figure 4. It is interesting to note that while $MgMH_{13}$ is the most stable cluster containing an odd number of hydrogen atoms for both transition metals, the most stable cluster with an even number of hydrogens is different for the two transition metals (i.e., $MgScH_{12}$ and $MgTiH_{10}$). We note that these most stable sizes are also close to the saturation limits of $MgScH_{13}$ and $MgTiH_{14}$.

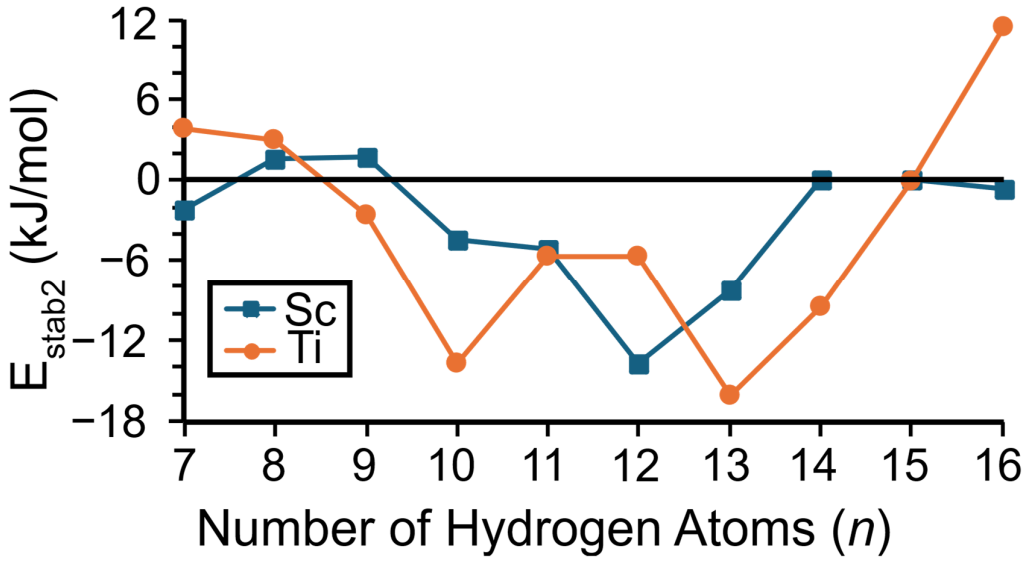


Figure 5. Plot of the second stabilization energy versus the number of hydrogen atoms in $MgMH_n$ clusters (n = 7–16), with the metal, M, being Sc (blue squares) and Ti (orange circles).

Lastly, a comment can be made comparing the partial charges of each transition metal in Tables 1 and 2. With only a few exceptions, the partial charges for magnesium in $MgMH_n$ are larger (more positive) when the transition metal in the cluster is titanium rather than scandium. In addition, scandium is more positively charged than titanium for all cluster sizes, and titanium is actually predicted for larger clusters to even be partially negatively charged.

4. Conclusions

A double-hybrid DFT approach is used for the first time to explore small $MgMH_n$ (M = Sc and Ti, n = 1–18) clusters, which serve as models to explore the internal bonding and properties of transition metal-doped magnesium hydride clusters. At this higher level of theory than has been previously considered, several differences with regard to the effect and role of the transition metal are noted. It is found that the hydrogen saturation limit in these clusters occurs at $MgScH_{13}$ and $MgTiH_{14}$, which have large 15.9% and 16.4%

hydrogen by mass, respectively. Additionally, the most stable clusters with an even and odd number of hydrogen atoms are found to be $MgScH_x$ (x = 12 and 13) and $MgTiH_y$ (y = 10 and 13). Overall, the distance between atoms is often larger at this higher level of theory for small clusters, but the Mg-M distance is almost exclusively smaller when utilizing this double-hybrid DFT method for larger clusters that contain more than six hydrogen atoms. For particular sizes, differences in the ground state structures are noted at this high DSDPBEP86/6-311++G(3df,3pd) double-hybrid level of theory.

Supplementary Materials: The following supporting information can be downloaded at: https://www.mdpi.com/article/10.3390/hydrogen7020077/s1. The supplementary data to this article include the determined Cartesian coordinates for the lowest energy $MgScH_n$ and $MgTiH_n$ (n = 1–18) clusters calculated at the DSDPBEP86/6-311++G(3df,3pd) level of theory. The supporting information also contains Table S1 (calculated binding energies), Table S2 (predicted H_2 stretching frequencies), and Figure S1 (highest occupied molecular orbitals) of select $MgMH_n$ clusters.

Funding: This study utilized the Advanced Cyberinfrastructure Coordination Ecosystem: Services and Support (ACCESS) supported by the National Science Foundation awards #2138259, 2138286, 2138307, 2137603, and 2138296. We performed these calculations on the Expanse high-performance computing cluster at the San Diego Supercomputing Center through grant allocation #CHE130094. We thank the Kentucky Academy of Science for financial support of this research through grant #64195005.

Data Availability Statement: The xyz Cartesian coordinates of each optimized global minimum structure shown in Figure 1 of this manuscript are provided in the Supplementary Materials. Additionally, the data presented in this study are available on request from the corresponding author.

Acknowledgments: We acknowledge Murray State University; the Jones College of Science, Engineering, and Technology; the Department of Chemistry; and the Committee on Institutional Studies and Research (CISR) for support of this research.

Conflicts of Interest: The author declares no conflicts of interest.

References

1. Koch, S.; Klitzman, R. Reliance on Fossil Fuels: Ethical Implications for Intensivists. *Intensive Care Med.* **2023**, *49*, 330–333. [CrossRef]
2. Solomon, C.G.; Salas, R.N.; Malina, D.; Sacks, C.A.; Hardin, C.C.; Prewitt, E.; Lee, T.H.; Rubin, E.J. Fossil-Fuel Pollution and Climate Change—a New Nejm Group Series. *N. Engl. J. Med.* **2022**, *386*, 2328–2329. [CrossRef] [PubMed]
3. Oramulu, I.; Paglioni, V.P. The Hydrogen Economy: Progress and Challenges to Future Growth. *Hydrogen* **2026**, *7*, 51. [CrossRef]
4. Dragassi, M.-C.; Royon, L.; Redolfi, M.; Ammar, S. Hydrogen Storage as a Key Energy Vector for Car Transportation: A Tutorial Review. *Hydrogen* **2023**, *4*, 831–861. [CrossRef]
5. Pistidda, C. Solid-State Hydrogen Storage for a Decarbonized Society. *Hydrogen* **2021**, *2*, 428–443. [CrossRef]
6. Cao, Z.; Habermann, F.; Burkmann, K.; Felderhoff, M.; Mertens, F. Unstable Metal Hydrides for Possible On-Board Hydrogen Storage. *Hydrogen* **2024**, *5*, 241–279. [CrossRef]
7. Nemukula, E.; Mtshail, C.B.; Nemangwele, F. Metal Hydrides for Sustainable Hydrogen Storage: A Review. *Int. J. Energy Res.* **2025**, *2025*, 6300225. [CrossRef]
8. Yartys, V.A.; Lototskyy, M.V.; Akiba, E.; Albert, R.; Antonov, V.E.; Ares, J.R.; Baricco, M.; Bourgeois, N.; Buckley, C.E.; Bellosta von Colbe, J.M.; et al. Magnesium based materials for hydrogen based storage: Past, present, and future. *Int. J. Hydrog. Energy* **2019**, *44*, 7809–7859. [CrossRef]
9. von Colbe, J.B.; Ares, J.-R.; Barale, J.; Baricco, M.; Buckley, C.; Capurso, G.; Galladat, N.; Grant, D.M.; Guzik, M.N.; Jacob, I.; et al. Application of hydrides in hydrogen storage and compression: Achievements, outlook and perspectives. *Int. J. Hydrog. Energy* **2019**, *44*, 7780–7808. [CrossRef]
10. Saeid, M.F.; Abdulkabir, B.A.; Ismail, M.; Setiabudi, H.D. Enhanced hydrogen storage properties of MgH_2 through doping with titanium-based catalyst materials: A review and bibliometric analysis. *Mater. Sci. Semicond. Process.* **2025**, *200*, 109931. [CrossRef]
11. Jangir, M.; Jain, I.P.; Mirabile Gattia, D. Effect of Ti-Based Additives on the Hydrogen Storage Properties of MgH_2: A Review. *Hydrogen* **2023**, *4*, 523–541. [CrossRef]

12. Kyoi, D.; Sato, T.; Rönnebro, E.; Kitamura, N.; Ueda, A.; Ito, M.; Katsuyama, S.; Hara, S.; Noréus, D.; Sakai, T. A new ternary magnesium-titanium hydride Mg_7TiH_x with hydrogen desorption properties better than both binary magnesium and titanium hydrides. *J. Alloys Compd.* **2004**, *372*, 213–217. [CrossRef]
13. Luo, X.; Grant, D.M.; Walker, G.S. Hydrogen storage properties of nano-structured $0.65MgH_2/0.35ScH_2$. *Int. J. Hydrog. Energy* **2013**, *38*, 153–161. [CrossRef]
14. Meng, Z.Q.; Liang, Y.M.; Li, F.Z.; Zhao, Y.R. DFT study on geometric, electronic, bonding and spectral properties of scandium-doped magnesium clusters. *Comput. Mater. Sci.* **2025**, *259*, 114187. [CrossRef]
15. Zhao, Z.; Xie, G.; Wang, N.; Hao, S.; Jia, Y. DFT study on structural, electronic, and magnetic properties of titanium-doped magnesium clusters Ti_2Mg_n. *Mol. Phys.* **2025**, *2025*, e2590145. [CrossRef]
16. Boruah, B.; Kalita, B. Role of 3d transition metal doping in determining the electronic structure and properties of small magnesium clusters: A DFT-based comparison of neutral and cationic states. *J. Nanopart. Res.* **2020**, *22*, 370. [CrossRef]
17. Chatterjee, S.; Bandyopadhyay, D. Hydrogen storage on MgO supported $TiMg_n$ (n = 2–6) clusters: A first principle investigation. *Int. J. Hydrog. Energy* **2024**, *77*, 1467–1475. [CrossRef]
18. Chatterjee, S.; Bandyopadhyay, D. Insights into the electronic structure and stability of $TiMg_n$ (n = 1–12) clusters: Validation of electron counting rule. *Mater. Today Commun.* **2022**, *32*, 103860. [CrossRef]
19. Bandyopadhyay, D.; Chatterjee, S.; Trivedi, R.; Dhaka, K. Insights into catalytic behavior of $TiMg_n$ (n=1–12) nanoclusters in hydrogen storage and dissociation process: A DFT investigation. *Int. J. Hydrog. Energy* **2022**, *47*, 13418–13429. [CrossRef]
20. Tang, Y.; Ding, L.-P.; Dou, X.-L.; Shao, P.; Wei, G.-D.; Guo, Y.-J.; Zeng, J.-H. Structures and Electronic and Hydrogen Storage Properties of Magnesium Scandium Hydrides. *Inorg. Chem.* **2022**, *61*, 15569–15575. [CrossRef]
21. Boruah, B.; Kalita, B. Alloying ratio versus cluster size for reversible hydrogen storage in 3d transition metal doped small Mg clusters: Dispersion corrected DFT study. *J. Energy Storage* **2023**, *72*, 108217. [CrossRef]
22. Lyon, J.T. Hydrogen Binding and Dissociation in $MgScH_n$ Clusters ($n \leq 20$). *Int. J. Hydrog. Energy* **2021**, *46*, 36872–36877. [CrossRef]
23. Newland, C.; Balamurugan, D.; Lyon, J.T. Structure and Properties of $MgTiH_n$ Clusters ($n \leq 20$). *Hydrogen* **2024**, *5*, 669–681. [CrossRef]
24. Lyon, J.T. Building Blocks: Investigating the Structures, Properties, and Reactivity of Strongly Bound Atomic Clusters at a PUI. In *Physical Chemistry Research at Undergraduate Institutions*; Hopkins, T., Parish, C.A., Eds.; ACS Books: Washington, DC, USA, 2022; Volume 2, Chapter 10; pp. 165–179. [CrossRef]
25. Chen, H.; Liang, H.; Dai, W.; Lu, C.; Ding, K.; Bi, J.; Zhu, B. $MgScH_{15}$: A highly stable cluster for hydrogen storage. *Int. J. Hydrog. Energy* **2020**, *45*, 32260–32268. [CrossRef]
26. Zhang, J.; Dolg, M. ABCLUSTER: The Artificial Bee Colony Algorithm for Cluster Global Optimization. *Phys. Chem. Chem. Phys.* **2015**, *17*, 24173–24181. [CrossRef] [PubMed]
27. Zhang, J.; Dolg, M. Global Optimization of Clusters of Rigid Molecules Using the Artificial Bee Colony Algorithm. *Phys. Chem. Chem. Phys.* **2016**, *18*, 3003–3010. [CrossRef]
28. Winkeler, M.; Richardson, C.N.; Carlin, R.; Lyon, J.T. Structural evolution of inorganic Si_nPd_2 (n = 1–17) clusters. *Chem. Inorg. Mater.* **2025**, *7*, 100121. [CrossRef]
29. Kozuch, S.; Martin, J.M.L. Spin-component-scaled double hybrids: An extensive search for the best fifth-rung functionals blending DFT and perturbation theory. *J. Comp. Chem.* **2013**, *34*, 2327–2344. [CrossRef] [PubMed]
30. McLean, A.D.; Chandler, G.S. Contracted Gaussian-basis sets for molecular calculations. 1. 2nd row atoms, Z=11–18. *J. Chem. Phys.* **1980**, *72*, 5639–5648. [CrossRef]
31. Raghavachari, K.; Trucks, G.W. Highly correlated systems: Excitation energies of first row transition metals Sc-Cu. *J. Chem. Phys.* **1989**, *91*, 1062–1065. [CrossRef]
32. Gimferrer, M.; Hasecke, L.; Bödecker, M.; Mata, R.A. Accurate vibrational hydrogen-bond shift predictions with multicomponent DFT. *Chem. Sci.* **2025**, *16*, 11002–11011. [CrossRef]
33. Bödecker, M.; Lwin, E.; Knüppe, F.; Evers, N.O.; Sennert, E.; Niessner, M.; Lüttschwager, N.O.B.; Martin, A.S. HyDRA-II: Spectroscopic results and BEsT guesses for the mono-and dihydrate blind challenge. *ChemRxiv* **2026**. *manuscript in preparation*. [CrossRef]
34. Martin, J.M.L.; Santra, G. Empirical Double-Hybrid Density Functional Theory: A 'Third Way' in Between WFT and DFT. *Isr. J. Chem.* **2020**, *60*, 787–804. [CrossRef]
35. Frisch, M.J.; Trucks, G.W.; Schlegel, H.B.; Scuseria, G.E.; Robb, M.A.; Cheeseman, J.R.; Scalmani, G.; Barone, V.; Petersson, G.A.; Nakatsuji, H.; et al. *Gaussian 16, Revision C.01*; Gaussian, Inc.: Wallingford, CT, USA, 2019.
36. Glendening, E.D.; Badenhoop, J.K.; Reed, A.E.; Carpenter, J.E.; Bohmann, J.A.; Morales, C.M.; Karafiloglou, P.; Landis, C.R.; Weinhold, F. *NBO 7.0.*; Theoretical Chemistry Institute, University of Wisconsin: Madison, WI, USA, 2018.

37. Strande, S.; Cai, H.; Tatineni, M.; Pfeiffer, W.; Irving, C.; Majumdar, A.; Mishin, D.; Sinkovits, R.; Norman, M.; Wolter, N. Expanse: Computing without Boundaries: Architecture, Deployment, and Early Operations Experiences of a Supercomputer Designed for the Rapid Evolution in Science and Engineering. In *PEARC'21: Practice and Experience in Advanced Research Computing 2021: Evolution Across All Dimensions*; Association for Computing Machinery: New York, NY, USA, 2021; Article No. 47; pp. 1–4. [CrossRef]
38. Boerner, T.J.; Deems, S.; Furlani, T.R.; Knuth, S.L.; Towns, J. ACCESS: Advancing Innovation: NSF's Advanced Cyberinfrastructure Coordination Ecosystem: Services & Support. In *Practice and Experience in Advance Research Computing (PEARC '23)*; Association for Computing Machinery: New York, NY, USA, 2023. [CrossRef]
39. Dennington, R.; Keith, T.A.; Millam, J.M. *GaussView*, version 6.0.16; Semichem Inc.: Shawnee Mission, KS, USA, 2016.
40. Dore, E.M.; Lyon, J.T. The Structures of Silicon Clusters Doped with Two Gold Atoms, Si_nAu_2 (n = 1–10). *J. Clust. Sci.* **2016**, *27*, 1365–1381. [CrossRef]
41. Liu, Q.; Liang, X.; Bao, X.; Meng, Y.; Hu, Y.; Zhang, M. The Structural Evolutions and Superatomic Properties of the Single-in-Atom-Doped Cu Clusters. *J. Clust. Sci.* **2026**, *37*, 23. [CrossRef]

Disclaimer/Publisher's Note: The statements, opinions and data contained in all publications are solely those of the individual author(s) and contributor(s) and not of MDPI and/or the editor(s). MDPI and/or the editor(s) disclaim responsibility for any injury to people or property resulting from any ideas, methods, instructions or products referred to in the content.